Desalination and Water Treatment
www.deswater.com

doi: 10.1080/19443994.2015.1043486

57 (2016) 10159–10168
May

Taylor & Francis
Taylor & Francis Group

Performance evaluation of solidification/stabilization of dredged sediment using alkali-activated slag

Han-na Cho, Jae-Ho Shim, Joo-Yang Park*

Department of Civil and Environmental Engineering, Hanyang University, 222 Wangsimni-ro, Seongdong-gu, Seoul, Republic of Korea, emails: hncho@kei.re.kr (H.-n. Cho), jaehoshim@hanyang.ac.kr (J.-H. Shim), Tel. +82 2 2296 7536; email: jooypark@hanyang.ac.kr (J.-Y. Park)

Received 15 January 2015; Accepted 15 April 2015

ABSTRACT

Fine dredged sediment was immobilized using ground granulated blast furnace slag as a new binder for supplementary cementitious materials in a 3.5% NaOH solution to study its solidification/stabilization (S/S) and uses in various industrial applications. The aim of this study is to compare effect of mixing conditions of the saturated-surface-dry of dredged sediment to determine the proper mixing method in the S/S process. Measurements of mechanical strength, heavy metal leachability, and microstructural characterization of the dredged sediment treated with alkali-activated slag (AAS) paste were carried out. The maximum value of the mechanical strength was obtained when the same amount of the NaOH solution as the saturated-surface-dry of the dredged sediment was added. The leaching experiment results showed that heavy metals were immobilized in the AAS paste, and that Cr, Cd, and Pb were not detected. The results of the analysis indicate the relationship between mechanical strength and (Ca + Na)/(Si + Al) ratio. This study demonstrates the possibility of successfully using fine dredged sediment as a base aggregate or a sub-base material for concrete production.

Keywords: Alkali-activated slag; Alkaline activator; Dredged sediment; Saturated-surface-dry; Solidification and stabilization

1. Introduction

Dredged sediment is excavated from the bottoms of lakes, rivers, estuaries, and marine locations in order to maintain existing navigation channels or in the construction of new port and harbor facilities. Dredge sediment is generally classified as waste that should ideally be reused in wetland restoration, capping, or construction applications. However, the pollutants in the sediments should be considered, including inorganic pollutants such as heavy metals including Cr, Cu, Cd, and Pb and organic pollutants such as polychlorinated biphenyl, tributyltin, total petroleum hydrocarbons, and chemical oxygen. Due to high water content, the presence of salts or organic matter, and low strength, these sediments cannot be used directly in concrete products. In addition, fine sediment (<75 μm) is commonly disposed of in landfills. It is difficult to reduce the contaminants from fine

*Corresponding author.

Presented at GMVP Desalination Academic Workshop, Seoul, Korea, December 9, 2014

sediment because of the strong bonds formed. In addition, although contaminants are reduced in the sediment, it is difficult to recycle fine sediment due to its small size and low strength.

Hence, solidification/stabilization (S/S) technology has been evaluated for the treatment of dredged sediment. One of the best ways to treat dredged sediment is S/S, which has three main advantages: (1) it is a simple process, (2) it can provide basic data for various applications such as construction, land creation, and capping, and (3) it may be more cost-effective than excavation and off-site disposal.

The binder for S/S is usually Portland cement (PC). The pore water of PC has a high pH in the range from 12.5 to 13.5 and limits the mobility of many heavy metals due to precipitation as hydroxides, increases their sorption onto cement mineral phases, and decreases solubility. However, the need for new binders, which are industrial by-products that can be utilized as supplementary cementitious materials (SCMs) such as ground granulated blast furnace slag (GGBFS) and fly ash (FA), has been rapidly increasing. SCMs are alkali-activated binders that are excellent alternative materials for cement. They significantly increase the sustainability of the binder and reduce the overall costs and environmental impact of PC. A low-energy process for the production of FA and GGBFS as industrial by-products is required in order to produce a substantial decrease in greenhouse gas emissions, especially CO_2 [1].

Interestingly, GGBFS can be hardened with a lower concentration of alkaline activator than FA. The different types of alkaline activators include (1) alkalis (e.g. MOH), (2) silicates (e.g. $M_2O{\cdot}nSiO_2$), (3) aluminates (e.g. $M_2O{\cdot}nAl_2O_3$), (4) non-silicate weak acid salts (e.g. M_2CO_3, M_3PO_4), (5) non-silicate strong acid salts (e.g. M_2SO_4), and (6) aluminosilicates (e.g. $M_2O{\cdot}nAl_2O_3{\cdot}nSiO_2$) [2].

To achieve high strength and good product quality, the binder type, water to binder ratio, and curing temperature are important factors. Among these factors, the water to binder ratio has been extensively studied [3–5]. Most researchers simply added more water when mixing with dried sludge or sediment in the solidification process because it is considered as a unifying condition and produces minimally varying results. However, this causes an increase in water to binder ratio and limits the results. Thus, a study to consider the handling of the water content of sludge or sediment is needed for the S/S process.

In this paper, the saturated-surface-dry of dredged sediment in the S/S process was evaluated based on the mechanical strength and microstructural characteristics. The used dredged sediment collected was the fine fraction of sediment smaller than 30 μm because dredged sediment larger than 75 μm has been used in practice. In addition, the calcination of dredged sediment was not studied for economic systems because related studies have already been carried out by other researchers. The concentration of alkaline solution was fixed using a 3.5% sodium hydroxide solution to confirm the availability of S/S for dredged sediment with a low concentration alkaline solution. The original dredged sediment and dried sediment were compared. In one case, the same amount of water as saturated-surface-dry of dredged sediment was added; in another case, the same amount of alkaline solution as saturated-surface-dry of dredged sediment was added. First, the samples were developed by testing the flexural/compressive strengths under various conditions including different water contents in the S/S process. Secondly, the stability of heavy metals was evaluated in samples cured for seven days. Lastly, the different mechanisms of S/S were evaluated using X-ray diffraction (XRD), field-emission scanning electron microscopy (FE-SEM), and Fourier transform infrared spectroscopy (FTIR).

2. Materials and methods

2.1. Materials

The dredged sediment was collected from the Nam harbor, near repair shipyard, Busan, South Korea, was black, and possessed a somewhat unpleasant smell due to the presence of organic matter. The physical characteristics and chemical compositions of the dried dredged sediment are reported in Tables 1 and 2. The dredged sediment was dried to a constant weight at 105°C for 4 h and then finely ground.

The major binder used in this study is GGBFS (POSCO, Korea), which is a third class material according to KS F2563. The chemical composition of GGBFS is shown in Table 3.

The alkaline activator was a fixed 3.5% NaOH solution made from analytical grade (>93%) sodium hydroxide beads (Showa Chemical Co., Ltd) and ultrapure water.

2.2. Experimental methods

2.2.1. Sample preparation

Natural dredged sediment and dried dredged sediment were prepared for this study. The dried dredged sediment was dried at 105°C for 4 h. The reaction of the dredged sediment in a 4% NaOH solution was performed before beginning the main

experiment. The main experiment was carried out according to ASTM C 305. The dredged sediment and GGBFS were mechanically premixed and then mixed with an activator solution at a water to binder ratio of 0.3 (binder: GGBFS + NaOH). In these cases, the important variable is the water content. In the first set of experiments, the dried dredged sediment was mixed with GGBFS and additional NaOH solution depending on the saturated-surface-dry of the dredged sediment. Secondly, the dried dredged sediment was mixed with GGBFS and NaOH solution with the same amount of water as of the saturated-surface-dry of the dredged sediment. Finally, natural dredged sediment was mixed with GGBFS. All mixtures were placed in molds (40 mm × 40 mm × 160 mm), sealed in plastic bags, and then cured at 60˚C for the first 24 h. The specimens were then removed from the molds and cured for 3, 7, or 28 d at 20 ± 1˚C. Table 4 shows the mixing design for AAS paste with dredged sediment specimens.

2.2.2. Sample analysis

The mechanical strength tests of the specimens were carried out according to ASTM C 348 and C 349 standards. First, the flexural strengths of the rectangular prisms (40 mm × 40 mm × 160 mm) were evaluated according to ASTM C 348. Second, compressive strength tests were carried out on the same specimens previously used for flexural strength tests according to ASTM C 349.

Toxicity characteristic leaching procedure (TCLP) tests were performed to examine the leaching characteristics of the specimens according to TCLP method 1311.

The microstructural characteristics of the specimens were evaluated on a Bruker AXS D5005 goniometer (Bruker, Germany) under the following conditions: Cu Kα radiation ($\lambda = 1.5406$ nm) and $2\theta = 5–70^{\circ}$ at a scanning rate of 2˚ per minute using XRD. The morphological characterization of the specimens was carried out on a SUPRA 55VP FE-SEM (Carl Zeiss, Germany) with a platinum powder coating applied by a sputter coater (BAL-TEC/SCD 005). The energy dispersive spectroscopy (EDS) plots were obtained over a specified region. FTIR spectroscopy using the KBr pellet method was performed in a Nicolet 6700 (Thermo Scientific, USA) by scanning 32 times from 4,000 to 400 cm^{-1} at a resolution of 4 cm^{-1}.

The XRD patterns of the samples were analyzed by comparison with those provided in The Joint Committee for Powder Diffraction Standards (JCPDS) for identification of the inorganic compounds.

3. Results and discussion

3.1. Mechanical strength

The reaction of dredged sediment with a 4% NaOH solution was tested to verify the hardenability as a binder before the main experiments. However, the dredged sediment mixed with 4% NaOH solution demonstrated no mechanical strength. Therefore, dredged sediment needs a binder for S/S, and the water to binder ratio was considered using GGBFS as the major binder and NaOH as an anhydrous binder.

The mechanical properties are the most important factors for S/S. In particular, for the utilization of dredged sediment, the flexural strength and compressive strength at 3, 7, and 28 d are delineated in Figs. 1 and 2, respectively. S1 had flexural and compressive strengths of 1.2 and 4.9 MPa, respectively, within three days and then leveled off. The reason for the initial high strength values was that the initial curing temperature was 60˚C for the first 24 h. In addition, the maximum compressive strength value was 6.4 MPa. S2 and S3 showed similar characteristics, but the strengths were lower than those of S1. S2 reacted at a lower alkaline activator concentration than S1. S3 reacted with not only a lower concentration of alkaline activator, but with a higher concentration of water compared to S1 and S2.

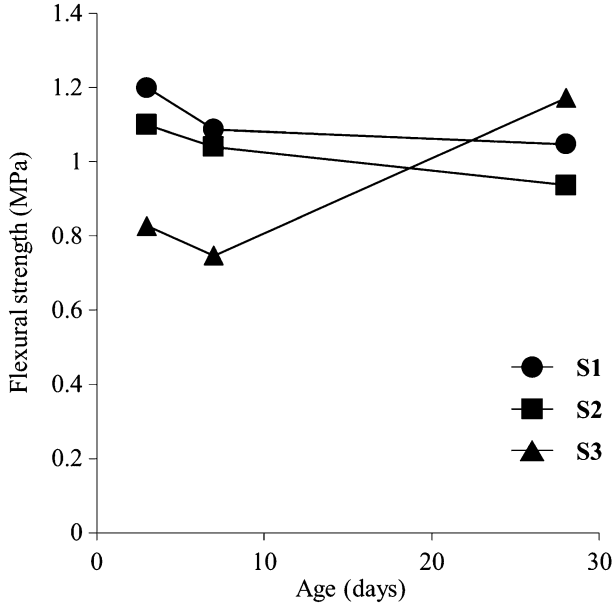

Fig. 1. The flexural strength of S1, S2 and S3.

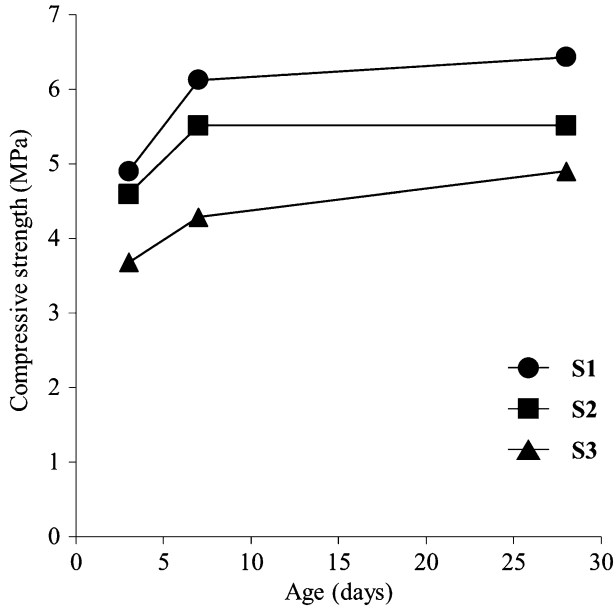

Fig. 2. The compressive strength of S1, S2 and S3.

3.2. Heavy metal leachability

Table 5 shows the results of the TCLP test. No heavy metals (Cu, Cr, Cd, and Pb) were detected in the dredged sediment treated with alkali-activated slag (AAS) paste. As a result, the immobilization efficiency was 99% or greater. It appears that these heavy metals were immobilized in the hardened AAS matrix by sorption onto the C–S–H (calcium silicate hydrate) surface [6,7]. These results imply that dredged sediment treated with AAS paste is suitable for beneficial reuse purposes such as concrete products.

3.3. Microstructural characterization

The XRD patterns of all of the samples are shown in Fig. 3. Although the masses of GGBFS, alkaline activator, and dredged sediment were the same, the XRD patterns show different peak patterns. However, the XRD patterns of all samples show typical C–S–H(I) [8,9] peaks with 2 peaks at 29.5 and 50.2 (JCPDS 84-0148). Additional phases include akermanite ($Ca_2MgSi_2O_7$, JCPDS 88-0777), gehlenite ($Ca_2Al(AlSi)O_7$, JCPDS 72-2128), $C_4A\underline{C}H_{11}$ ($3CaO{\cdot}Al_2O_3{\cdot}CaCO_3{\cdot}11H_2O$, JCPDS 41-0219), hydrotalcite ($Mg_6Al_2(CO_3)(OH)_{16}{\cdot}4(H_2O)$, JCPDS 41-1428), and quartz (SiO2, JCPDS 87-2096). The presence of C–S–H phase is evident in all of the hardened samples and is typically associated with mechanical strength as it is one of the main reaction products of AAS [10–16]. The major C–S–H phase peaks should appear with a background peak in the 2 range of 25–35° [8] due to its semi-amorphous nature. Riversideite ($Ca_5Si_6O_{16}(OH)_2{\cdot}2(H_2O)$) and rustumite ($Ca_{10}(Si_2O_7)_2(SiO_4)Cl_2(OH)_2$) were represented by similar peak patterns to the C–S–H(I) phases. Riversideite is one of the hydration products of AAS [17] and had characteristics peaks at 2 values of 28.8, 29.5, and 31.1 (d = 3.17, 3.02, and 2.87 Å, respectively). Rustumite as a calcium silicate hydroxide mineral contains chlorine, whose structure was

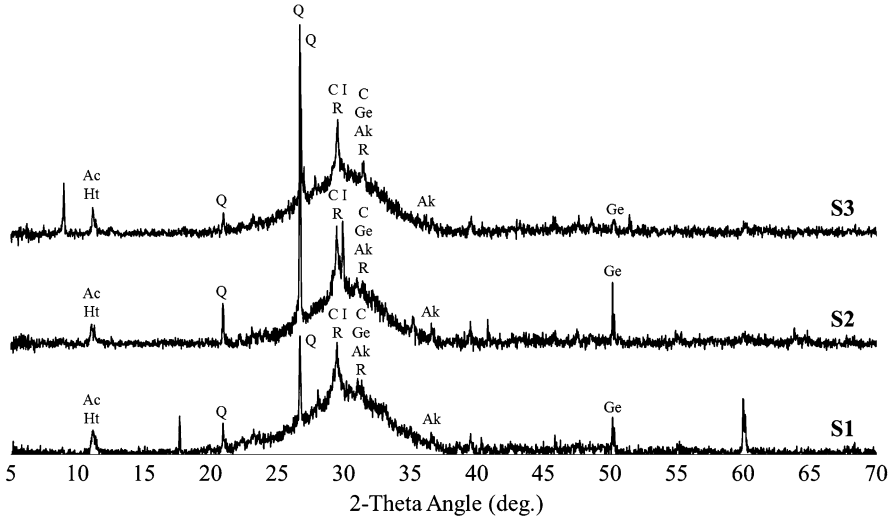

Fig. 3. XRD patterns of S1, S2 and S3. Ac—$C_4A\underline{C}H_{11}$, Ht—hydrotalcite, Q—quartz, CI—C–S–H (I), R—rustumite, C—C–S–H, Ge—gehlenite, Ak—akermanite.

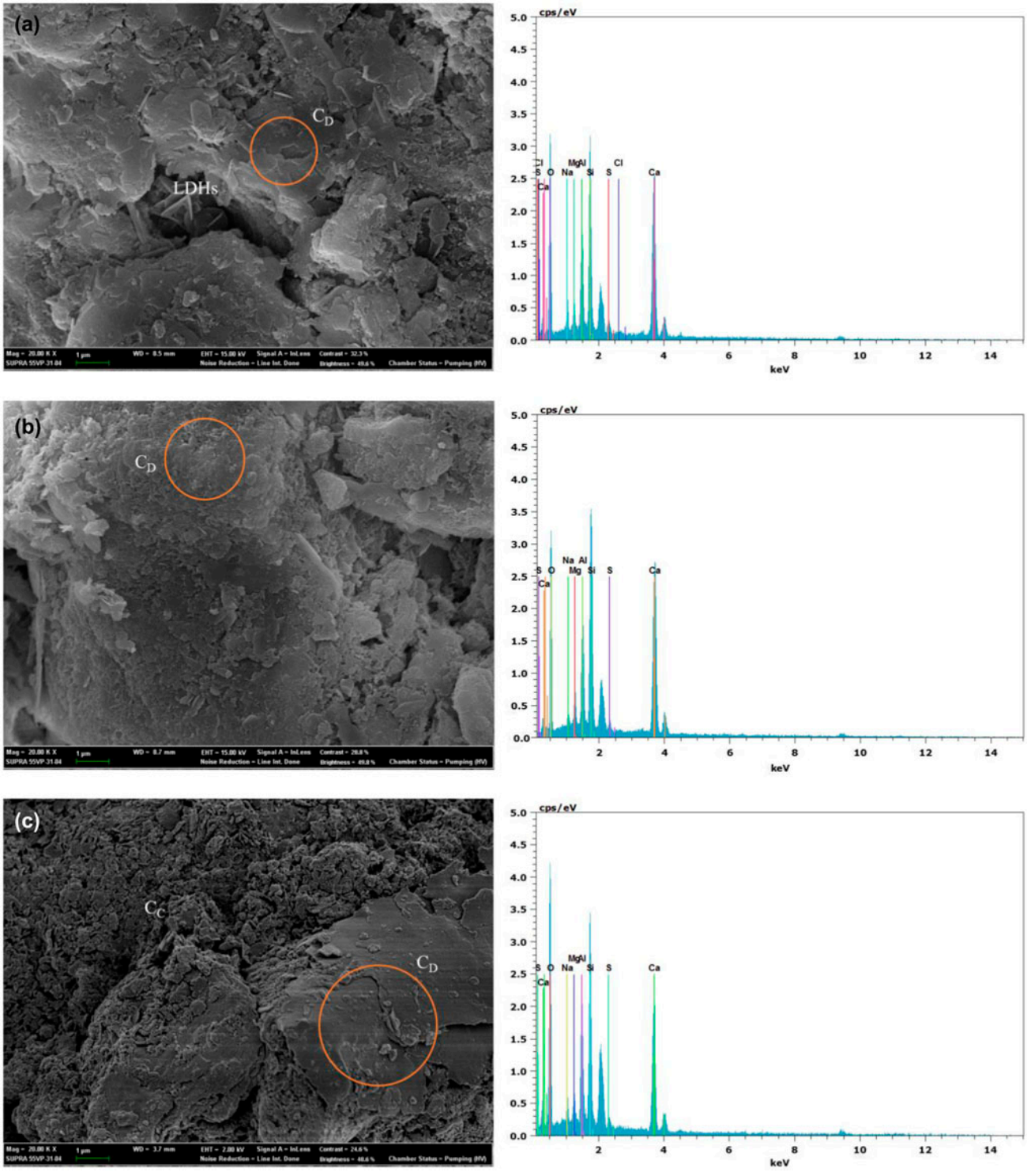

Fig. 4. FE-SEM micrographs and EDS spectrums of (a) S1, (b) S2 and (c) S3.

formed by chlorine contained in the dredged sediment. Chlorine from dredged sediment exists in the inner pores and on the surface of dredged sediment.

Akermanite and gehlenite series are mineral phases and the most important group members of the melilite group. These two phases were found in all of

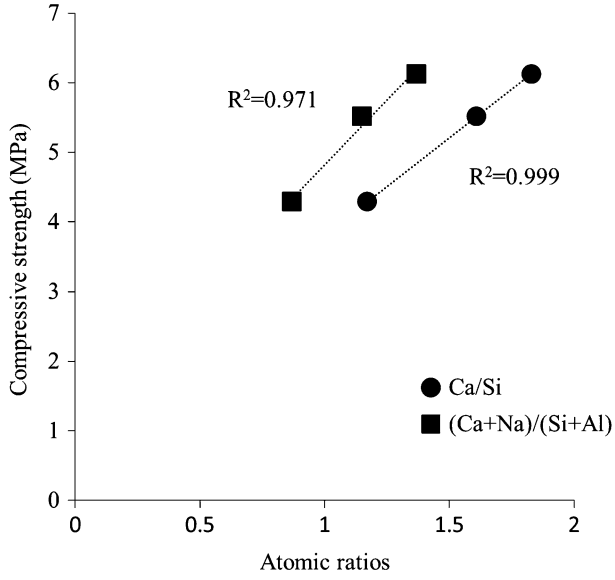

Fig. 5. Compressive strength as a function of atomic ratios: ● Ca/Si molar ratio, ■ (Ca + Na)/(Si + Al) molar ratio.

the samples and have been reported to exist in a crystalline form as a solid solution in unreacted raw GGBFS and paste [11–14,16]. The akermanite is uniaxial positive, and gehlenite is optically uniaxial negative [18,19]. Gehlenite has often been reported in NaOH-activated GGBFS with a high Al_2O_3 content [8].

$C_4A\underline{C}H_{11}$ and hydrotalcite are layered double hydroxide minerals with CO_3^{2-} in the interlayer. These two phases are difficult to distinguish in XRD patterns because they have the same layer spacing of 7.8 Å and are trigonal-hexagonal scalenohedral in the crystal system. S3 shows the highest peak intensity of $C_4A\underline{C}H_{11}$ and hydrotalcite among the samples. The seawater in the S3 dredged sediment contains carbonate, which consists of $C_4A\underline{C}H_{11}$ and hydrotalcite. Quartz is the most common sedimentary mineral.

Fig. 4 shows FE-SEM micrographs combined with the EDS microanalysis at a high magnification (20,000×). The FE-SEM micrographs illustrate the complex structures formed by the reactions of AAS with sediment particles. The materials appeared to be C–S–H phases and hexagonal-shaped crystals. C–S–H and LDHs phases were identified including C–S–H type D, C–S–H type C, and LDHs phases. In 1976, Diamond distinguished four morphological types of C–S–H on FE-SEM of fracture surfaces of cement pastes [8]. Type I is a fibrous material with fibers up to 2 μm long. Type II can be described as forming reticular networks or honeycombs. Type III is more massive and appears as small spheres. Type IV is more featureless and massive [8]. In this paper, Type III and Type IV are expressed as Type C and Type D, respectively. In all samples, we observed C–S–H type D, which was a more featureless and massive form. The presence of C–S–H was determined in the EDS spectra. The EDS spectrum reveals a majority of Ca and Si with trace amounts of Al and Na, and it indicates the Ca/Si ratio of C–S–H with Al and Na incorporation. As the structure of the C–S–H phases was modified by the presence of Na atoms [20,21], some of the Na ions will be incorporated into C–S–H, either replacing Ca ions to form N–C–S–H [22,23] or as charge balancers to compensate the substitution of Si^{4+} with Al^{3+} [24–26]. The type of C–S–H was characterized by Ca/Si ratio, which typically ranges from 0.7 to 2.3 [27]. A relationship between compressive strength and Ca/Si ratio of C–S–H was generally reported for activated slag systems [28]. In addition, the calculation of (Ca + Na)/(Si + Al) molar ratio was based on the Ca/Si molar ratio of C–S–H in Table 6. Fig. 5 shows the Ca/Si ratio and (Ca + Na)/(Si + Al) ratio as a function of compressive strength. The increase in compressive strength was explicitly related to the increases in Ca/Si ratio and (Ca + Na)/(Si + Al) ratio of C–S–H. Therefore, it is important to estimate the properties of the AAS paste using mineral components to predict the type of C–S–H. Similarly, we analyzed the OH/Ca ratio and OH/(Ca + Na) ratio using EDS. Hydroxide bonds are known to be crucial in determining the local microstructure of C–S–H [29–31]. The OH/Ca and OH/(Ca + Na) ratios overall show good agreement with the mechanical strength and structural characteristics. It seems that the decrease in OH^- groups due to interactions with Ca and Na is related to the increase in compressive strength. S1 and S2 have the same mass of water in the alkaline activator as a result of adding water in consideration of the water content of the dredged sediment. The values of the OH/Ca ratio for S1 and S2 are similar, with values of 3.8 and 3.9, respectively. On the contrary, the value for S3 is 5.9 due to the larger amount of water in the dredged sediment treated with AAS paste based on the higher mass of water compared to the saturated-surface-dry of the sediment.

The infrared spectra of the dredged sediment treated with AAS paste are illustrated in Fig. 6. The main broad band at 960–961 cm^{-1} is assigned to asymmetric stretching vibrations of Si–O–Si and Al–O–Si bonds originating from individual tetrahedral TO_4 (T=Si, Al) [32] that comprise C-(A)–S–H. In addition, the band at 491–509 cm^{-1} is assigned to O–Si–O bending vibrations [33]. Vibrations assigned to stretching of O–H and bending of H–O–H are observed around 3,400 and 1,650 cm^{-1}, respectively [34,35]. Traces of carbonates are associated with the asymmetric stretching

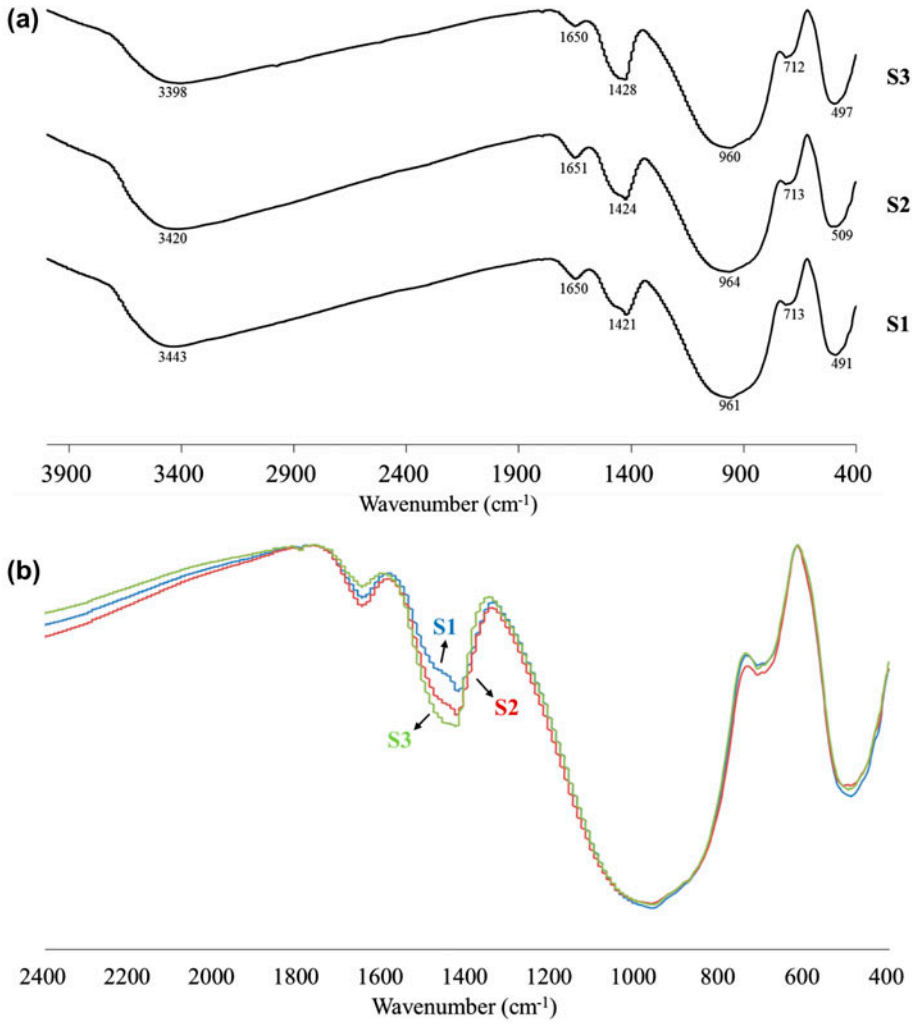

Fig. 6. FTIR spectra of S1, S2 and S3: (a) at regular intervals, (b) at overlapping.

Table 1
Physical characteristics of dredged sediment

Parameters		Values
Water content (%)		41
Absolute density (g cm^{-3})		2.744
Particle size classification (%)	Gravel	0.48
	Sand	95.065
	Silt	4.455
	Clay	0

mode of the O–C–O bonds of the CO_3^{2-} groups observed at 1,421–1,428 cm^{-1} and around 713 cm^{-1} [36–38]. The band of Si–O stretching and OH bending (Si–OH) [34] is also observed around the 850 cm^{-1} shoulder. As shown in Fig. 6, the width and intensity of the major band associated with the Si–O(Al) stretching vibrations in TO_4 tetrahedra around 960 cm^{-1} are the same for all of the samples. This confirms that these materials are similarly disordered and have the same mean chain length (MCL) of aluminosilicate polymers. On the other hand, around 1,424 cm^{-1}, the

Table 2
Heavy metals and organic contents of dredged sediment

Cr (mg L^{-1})	Cu (mg L^{-1})	Cd (mg L^{-1})	Pb (mg L^{-1})	TOC (%)
1,043	1,206.7	1.6	232	6.0

Table 3
Chemical compositions of GGBFS (%)

CaO	SiO_2	Al_2O_3	MgO	SO_3	TiO_2	Fe_2O_3	Others
46.2	32.3	13.5	3.2	2.0	1.0	0.4	1.4

Table 4
Composition of AAS paste with dredged sediment specimens

			Water (g)			
Sample labels	Slag (g)	Sediment (g)	W_{AA}	W_{SSD}	W_{DS}	NaOH (g)
S1	1,350	150	409.46	42	–	17.61
S2	1,350	150	409.46	42	–	15.97
S3	1,350	234.4	409.46	–	84.4	15.97

Notes: W_{AA}: water in proportion to 3.5% NaOH alkaline activator; W_{SSD}: added water in proportion to saturated-surface-dry; W_{DS}: water in dredged sediment.

Table 5
TCLP results of dredged sediment treated with AAS paste cured during 7 d

Sample labels	Cr (mg L^{-1})	Cu (mg L^{-1})	Cd (mg L^{-1})	Pb (mg L^{-1})
S1	ND	0.007	ND	ND
S2	ND	0.006	ND	ND
S3	ND	0.006	ND	ND
MDL	0.003	0.001	0.0007	0.001

Notes: ND: not detected; MDL: minimum detection limit.

Table 6
Average content of main elements in the matrix of S1, S2, and S3 and their ratios, detected by EDS

	Weight (atomic %)					Compositional coefficent	
Sample labels	OH	Ca	Si	Al	Na	Ca/Si	(Ca + Na)/(Si + Al)
S1	65.62	17.12	9.35	4.36	1.65	1.83	1.37
S2	65.04	16.81	10.42	4.91	0.85	1.61	1.15
S3	68.80	11.62	9.89	5.64	1.87	1.17	0.87

intensity of S3 is the highest among the samples because CO_2 is already dissolved in the dredged sediment.

4. Conclusions

GGBFS was activated using a 3.5% NaOH solution for immobilization of fine dredged sediment smaller than 30 μm. The following details were considered in this study: (1) the use of fine sediment, (2) the use of GGBFS as a by-product, which is an alternative cementitious material, and (3) the use of a low concentration of alkaline activator to improve cost-effectiveness. Finally, in this study, we focused on the saturated-surface-dry of dredged sediment in S/S and evaluated the mechanical strength and microstructural characteristics. Furthermore, the ability to use fine dredged sediment as a base aggregate or as a sub-base material was demonstrated. In terms of mechanical strength and heavy metal leachability, good behavior was confirmed. The dredged sediment treated with AAS paste had good compressive strength that

quickly achieved a high value due to the initial curing at 60˚C. The greatest mechanical strength was obtained when adding the same amount of NaOH solution as the saturated-surface-dry of the dredged sediment. Moreover, Cr, Cd, and Pb were not detected. XRD, SEM-EDS, and FTIR analyses revealed the presence of C–S–H as the major binding phase in AAS paste with dredged sediment. The results of the analysis show the relationship between mechanical strength and (Ca + Na)/(Si + Al) ratio. In addition, CO_2 and Cl^- from the inner water pores and surface of the dredged sediment were formed in the structure of the AAS paste. The comparisons depending on the mixing conditions using the water content of dredged sediment demonstrate a proper mixing method of dredged sediment in the S/S process and base data for use in various applications.

Acknowledgment

This research was supported by a grant (code 13IFIP-B065893-01) from the Industrial Facilities & Infrastructure Research Program funded by Ministry of Land, Infrastructure and Transport of the Korean government.

References

[1] E.M. Gartner, D.E. Macphee, A physico-chemical basis for novel cementitious binders, Cem. Concr. Res. 41 (2011) 736–749.
[2] V.D. Glukhovsky, Slag-Alkali Concretes Produced from Fine-Grained Aggregate, Vishchaya Shkola, Kiev, 1981.
[3] B. Felekoglu, S. Turkel, B. Baradan, Effect of water/cement ratio on the fresh and hardened properties of self-compacting concrete, Build. Environ. 42 (2007) 1795–1802.
[4] H. Justnes, A. Van Gemert, F. Verboven, E.J. Sellevold, Total and external chemical shrinkage of low w/c ratio cement pastes, Adv. Cem. Res. 8 (1996) 121–126.
[5] J. Schulze, Influence of water-cement ratio and cement content on the properties of polymer-modified mortars, Cem. Concr. Res. 29 (1999) 909–915.
[6] S. Bouzalakos, A.W.L. Dudeney, C.R. Cheeseman, Controlled low-strength materials containing waste precipitates from mineral processing, Miner. Eng. 21 (2008) 252–263.
[7] X.G. Li, Y. Lv, B.-G. Ma, Q.-B. Chen, X.-B. Yin, S.-W. Jian, Utilization of municipal solid waste incineration bottom ash in blended cement, J. Clean. Prod. 32 (2012) 96–100.
[8] H.F.W. Taylor, Cement Chemistry, second ed., Thomas Telford, 1997.
[9] H.F.W. Taylor, Nanostructure of C–S–H: Current status, Adv. Cem. Based Mater. 1 (1993) 38–46.
[10] A.H. Lav, M.A. Lav, Microstructural development of stabilized fly ash as pavement base material, J. Mater. Civ. Eng. 12 (2000) 157–163.
[11] J.I. Escalante-García, A.F. Fuentes, A. Gorokhovsky, P.E. Fraire-Luna, G. Mendoza-Suarez, Hydration products and reactivity of blast-furnace slag activated by various alkalis, J. Am. Ceram. Soc. 86 (2003) 2148–2153.
[12] J.G.S. Van Jaarsveld, J.S.J. Van Deventer, L. Lorenzen, The potential use of geopolymeric materials to immobilise toxic metals: Part I. Theory and applications, Miner. Eng. 10 (1997) 659–669.
[13] M.B. Haha, B. Lothenbach, G. Le Saout, F. Winnefeld, Influence of slag chemistry on the hydration of alkali-activated blast-furnace slag—Part II: Effect of Al_2O_3, Cem. Concr. Res. 42 (2012) 74–83.
[14] M. Ben Haha, G. Le Saout, F. Winnefeld, B. Lothenbach, Influence of activator type on hydration kinetics, hydrate assemblage and microstructural development of alkali activated blast-furnace slags, Cem. Concr. Res. 41 (2011) 301–310.
[15] M. Choquette, M.-A. Bérubé, J. Locat, Mineralogical and microtextural changes associated with lime stabilization of marine clays from eastern Canada, Appl. Clay Sci. 2 (1987) 215–232.
[16] S.D. Wang, K.L. Scrivener, Hydration products of alkali activated slag cement, Cem. Concr. Res. 25 (1995) 561–571.
[17] M. Brito, E. Case, W.M. Kriven, J. Salem, D. Zhu, Developments in Porous, Biological and Geopolymer Ceramics, Wiley, 2008.
[18] D.R. Waldbaum, J.A. Woodhead, Thermodynamic and crystallographic properties related to Al–Si–Mg ordering in $Ca_2MgSi_2O_7$–$Ca_2Al_2SiO_7$ melilite crystalline solutions, Fortschr. Miner. (1975) 119–131.
[19] M. Fleischer, R.E. Wilcox, J.J. Matzko, Microscopic determination of the nonopaque minerals, US Geological Survey Bulletin (1984).
[20] D. Dimas, I. Giannopoulou, D. Panias, Polymerization in sodium silicate solutions: A fundamental process in geopolymerization technology, J. Mater. Sci. 44 (2009) 3719–3730.
[21] S. Song, D. Sohn, H.M. Jennings, T.O. Mason, Hydration of alkali-activated ground granulated blast furnace slag, J. Mater. Sci. 35 (2000) 249–257.
[22] A. Palomo, A. Fernandez-Jimenez, G. Kovalchuk, L.M. Ordonez, M.C. Naranjo, Opc-fly ash cementitious systems: study of gel binders produced during alkaline hydration, J. Mater. Sci. 42 (2007) 2958–2966.
[23] C. Shi, P.V. Krivenko, D. Roy, Alkali-Activated Cements and Concretes, Taylor and Francis, 2006.
[24] A. Fernandez-Jimenez, F. Puertas, I. Sobrados, J. Sanz, Structure of calcium silicate hydrates formed in alkaline-activated slag: Influence of the type of alkaline activator, J. Am. Ceram. Soc. 86 (2003) 1389–1394.
[25] L.D. Mitchell, J.C. Margeson, J.J. Beaudoin, Synthesis and characterisation of lithium and sodium doped C–S–H, 12th International Congress on the Chemistry of Cement, Montreal, 2007, pp. 1–17.
[26] S.A. Bernal, R. Mejía de Gutiérrez, A.L. Pedraza, J.L. Provis, E.D. Rodriguez, S. Delvasto, Effect of binder content on the performance of alkali-activated slag concretes, Cem. Concr. Res. 41 (2011) 1–8.

[27] V.S. Ramachandran, J.J. Beaudoin, Handbook of Analytical Techniques in Concrete Science and Technology, William Andrew Publishing, LLC, 2000.
[28] M.M. Komljenovic, Z. Bascarevic, N. Marjanovic, V. Nikolic, Decalcification resistance of alkali-activated slag, J. Hazard. Mater. 233 (2012) 112–121.
[29] J.J. Chen, J.J. Thomas, H.F.W. Taylor, H.M. Jennings, Solubility and structure of calcium silicate hydrate, Cem. Concr. Res. 34 (2004) 1499–1519.
[30] J.J. Thomas, J.J. Chen, H.M. Jennings, D.A. Neumann, Ca−OH bonding in the C−S−H gel phase of tricalcium silicate and white portland cement pastes measured by inelastic neutron scattering, Chem. Mater. 15 (2003) 3813–3817.
[31] X. Cong, R.J. Kirkpatrick, ^{29}Si MAS NMR study of the structure of calcium silicate hydrate, Adv. Cem. Mater. 3 (1996) 144–156.
[32] A. Fernandez-Jimenez, A. Palomo, Mid-infrared spectroscopic studies of alkali-activated fly ash structure, Microporous Mesoporous Mater. 86 (2005) 207–214.
[33] J.W. Phair, J.S.J. Van Deventer, Effect of the silicate activator pH on the microstructural characteristics of waste-based geopolymers, Int. J. Miner. Process 66 (2002) 121–143.
[34] T. Uchino, T. Sakka, K. Hotta, M. Iwasaki, Attenuated total reflectance Fourier-transform infrared spectra of a hydrated sodium soilicate glass, J. Am. Ceram. Soc. 72 (1989) 2173–2175.
[35] T. Uchino, T. Sakka, M. Iwasaki, Interpretation of hydrated states of sodium silicate glasses by infrared and Raman analysis, J. Am. Ceram. Soc. 74 (1991) 306–313.
[36] F.B. Reig, J.V.G. Adelantado, M. Moreno, FTIR quantitative analysis of calcium carbonate (calcite) and silica (quartz) mixtures using the constant ratio method. Application to geological samples, Talanta 58 (2002) 811–821.
[37] M. Yousuf, A. Mollah, T.R. Hess, Y.N. Tsai, D.L. Cocke, An FTIR and XPS investigations of the effects of carbonation on the solidification/stabilization of cement based systems-Portland Type V with zinc, Cem. Concr. Res. 23 (1993) 773–784.
[38] P. Yu, R.J. Kirkpatrick, B. Poe, P.F. McMillan, X.D. Cong, Structure of calcium silicate hydrate (C–S–H): Near-, mid-, and far-infrared spectroscopy, J. Am. Ceram. Soc. 82 (1999) 742–748.